ORIGINAL RESEARCH

MR Imaging, MR Spectroscopy, and Diffusion Tensor Imaging of Sequential Studies in Neonates with Encephalopathy

A.J. Barkovich
S.P. Miller
A. Bartha
N. Newton
S.E.G. Hamrick
P. Mukherjee
O.A. Glenn
D. Xu
J.C. Partridge
D.M. Ferriero
D.B. Vigneron

BACKGROUND: Although the imaging, spectroscopic, and diffusion characteristics of brains of infants with neonatal encephalopathy have been described, the time course during which these changes evolve is not clear. The results of sequential MR imaging studies—including anatomic MR imaging, proton MR spectroscopy, and diffusion tensor imaging (DTI)—of 10 patients enrolled prospectively in a study of neonatal encephalopathy are reported to help to clarify the time course of changes in different brain regions during the first 2 weeks of life.

METHODS: Ten neonates were prospectively enrolled in a study of the evolution of MR findings in neonatal encephalopathy and were studied 2 (8 patients) or 3 (2 patients) times within the first 2 weeks of life. The MR examination included spin-echo T1 and T2-weighted images, DTI, and long echo time (288 milliseconds) proton MR spectroscopy. Diffusion parameters (diffusivity [D_{av}], fractional anisotropy [FA], and individual eigenvalues) were calculated for 10 1-cm^2 regions of interest in each hemisphere that were placed based on anatomic landmarks. D_{av} and FA were then measured manually in the same areas on a workstation. Metabolite ratios (NAA/Ch, Cr/Ch, Cr/NAA, Lac/Ch, and Lac/NAA) were calculated in 7 regions of interest. Imaging appearance, diffusion parameters, and metabolite ratios were then evaluated longitudinally (comparing with other studies on the same patient at different times) and cross-sectionally (comparing all studies performed on the same postnatal day).

RESULTS: In most of the patients a characteristic evolution of DTI and MR spectroscopy parameters was seen during the first 2 weeks after birth. Although the anatomic images were normal or nearly normal on the first 2 days after birth in most patients, abnormalities were detected on DTI (both visually and by quantitative interrogation of D_{av} maps) and proton MR spectroscopy (abnormal metabolite ratios). These parameters tended to worsen until about day 5 and then normalize, though in several patients abnormal metabolite ratios persisted. Of interest, as areas of abnormal diffusivity pseudonormalized within one region of the brain they would develop in other areas. Therefore, the pattern of injury looked very different when imaging was performed at different times during this evolution.

CONCLUSION: Patterns of injury detected by standard anatomic imaging sequences, DTI sequences, and proton MR spectroscopy varied considerably during the first 2 weeks after injury. The appearance of new areas of reduced diffusion simultaneous with the pseudonormalization of areas that had reduced diffusion at earlier times can result in an entirely different pattern of injury on diffusivity maps acquired at different time points. Awareness of these evolving patterns is essential if studies are performed and interpreted during this critical period of time.

During the past 15 years, MR techniques—including MR imaging, diffusion tensor imaging (DTI), and proton MR spectroscopy—have become the tools of choice in the study of brain injury in term neonates.[1-23] It has become clear that MR techniques are the most sensitive imaging techniques for detecting brain injury and that there is good association between MR findings and neurodevelopmental outcome.[24-29] Moreover, MR imaging can identify encephalopathic neonates at greatest risk for abnormal outcome.[29] With the advent of new techniques for therapy on perinatal and neonatal injury such as head cooling and pharmacological methods,[30-32] early assessment of the brain by MR techniques may serve as a decision point in determining whether intervention is indicated and, perhaps, what type of intervention. Therefore, it is critical to understand the evolution of early changes in the injured brain. As part of a prospective study of MR in perinatal and neonatal brain injury, 10 patients have been studied sequentially by standard MR imaging, DTI, and proton MR spectroscopy in the early postnatal period, with the first examination being performed in the first 48 hours in all cases. Of interest, the pattern of injury evolved continuously during the first 2 weeks after birth on all techniques. The evolving patterns are described and discussed in this manuscript.

Received July 21, 2005; accepted August 3.

From the Departments of Radiology (A.J.B., P.M., O.A.G., D.X., D.B.V.), Pediatrics (A.J.B., S.P.M., N.N., S.E.G.H., J.C.P., D.M.F.), and Neurology (A.J.B., S.P.M., A.B., D.M.F.), University of California at San Francisco, San Francisco, Calif.

This research was supported by the National Institutes of Health (grant P50 NS35902). These studies were carried out in part in the Pediatric Clinical Research Center, University of California, San Francisco, with funds provided by the National Center for Research Resources (grant 5 M01 RR-01271), U.S. Public Health Service.

Address correspondence to A. James Barkovich, MD, Neuroradiology Section, Department of Radiology, University of California at San Francisco, 505 Parnassus Ave, Room L371, San Francisco, CA 94143-0628.

Patients and Methods

Currently, 6151 consecutive term and near-term babies admitted to our neonatal intensive care unit have been prospectively screened as part of an ongoing study investigating the utility of neonatal brain MR imaging in assessing brain injury of neonates with neonatal encephalopathy. As the imaging characteristics of neonatal injury are well described in the literature, the protocol has recently been modified to better appreciate the early features of injury and, in particular, the changing anatomic MR imaging, DTI, and proton MR spectroscopy characteristics of the neonatal brain as the injury evolves. For this part

of the study, 802 babies were screened, 34 had exclusion criteria, 14 met entry criteria, 4 declined participation (via their parents) after initially enrolling in the study, and 10 (8 boys and 2 girls) were enrolled and studied after their parents gave informed consent. Entry criteria for this study are overt neonatal encephalopathy as assessed by a neonatologist or (1) umbilical artery pH $<$7.1; (2) umbilical artery base deficit $>$10; or (3) 5-minute Apgar score $\leq$5. Babies with suspected or confirmed metabolic disorders, congenital malformations, or congenital infections and babies born before 36 weeks' gestational age were excluded. Normative data were acquired from a cohort of 16 neonates who were recruited from our obstetrics clinic as a part of this study. All underwent this same MR study during the first week of life. The protocol was approved by the human research committee at our institution. Participation in the study was voluntary; the babies were studied only after informed consent was granted by their parents. Of the 10 patients reported in this study, 8 babies were studied twice and 2 were studied 3 times. The first studies were performed as soon as the neonate was judged sufficiently stable by the attending neonatologist. Subsequent studies were performed at times determined by the clinical condition of the neonate, the availability of MR scanner time, and the availability of personnel to accompany the neonate to the scanner. Scans performed within and including the first 24 hours after birth we considered to be performed on day 1 of life, those performed from 24–48 hours were considered as day 2, those from 48–72 hours as day 3, etc.

All patients except one (patient 195) were given final diagnoses of neonatal encephalopathy secondary to global hypoxic-ischemic incident. Patient 195 had a normal neonatal course, was delivered vaginally without complications, and was sent to the well-baby nursery, where he was judged "jittery." Mild hypoglycemia was noted and treated. Neonatal arterial blood gases showed a pH of 7.08, which qualified the baby for admission to this study and the parents consented to participate. The cause for this baby's signs was not ascertained. The other patients in the study all had complicated deliveries and early postnatal seizures (Table 1). The late prenatal courses of 2 of the subjects were complicated by maternal hypotension, one because of maternal sepsis and the other because of hypotension after epidural placement. Both infants were subsequently born by emergency cesarean section. One child started to seize in utero 3 days before delivery and was delivered emergently after a flat fetal heart rate was detected. The cause of the prenatal seizures was not determined. (Table 1 provides more details of the clinical courses.)

All studies were performed by using a custom-built MR-compatible neonatal incubator and a high-sensitivity specialized neonatal head coil to reduce patient motion, increase patient safety and comfort, and improve signal intensity-to-noise ratio (SNR) of the MR images.[33] During scanning, neonatologists monitored the infants and hand-ventilated intubated neonates. Infants were fed before scanning to avoid sedation whenever possible; sedation was used in 8 of the 22 MR images (36%). By using a 1.5T Signa EchoSpeed scanner (GE Medical Systems, Milwaukee, Wis), we performed an MR examination consisting of axial T2-weighted dual spin-echo (TR, 3000 milliseconds; TE, 60/120 milliseconds; 4-mm section thickness) and axial spin-echo (TR, 500 milliseconds; TE, 11 milliseconds; 4-mm section thickness) with an 18-cm field of view (FOV) and a 192 $\times$ 256 acquisition matrix. Each of these scans was evaluated separately by 2 pediatric neuroradiologists with experience in neonatal brain MR imaging, who assessed them for the presence and location of any signal intensity abnormalities in the thalami, corticospinal tracts, basal ganglia, cerebral cortex, cerebral white matter, and brain stem. Consensus was reached on all findings. Agreement was high between the 2 reviewers, with kappa value of 90%.

We used a multisection spin-echo single-shot echo-planar sequence to perform DTI (TR, 7000 milliseconds; TE, 99.5 milliseconds; 3-mm section thickness; no gap; 3 repetitions per image; with 18 $\times$ 36 cm FOV and 128 $\times$ 256 acquisition matrix), acquiring axial images through the whole brain with an in-plane resolution of 1.4 $\times$ 1.4 mm^2.[34-36] We acquired 7 images per axial section, including a T2-weighted reference image (b = 0 seconds/mm^2) and 6 diffusion-weighted images (b = 700 seconds/mm^2) in noncollinear gradient directions. The MR data were transferred to off-line workstations for postprocessing. From the DTI data, we computed the average diffusivity (D_{av}, also called apparent diffusion coefficient [ADC]), fractional anisotropy (FA), and the 3 eigenvalues of the diffusion tensor (λ_1, λ_2, and λ_3, in decreasing order of magnitude) bilaterally in the basal ganglia, ventrolateral thalami, posterior limbs of the internal capsules, corticospinal tracts in the centrum semiovale, frontal watershed white matter, parietal watershed white matter, calcarine cortex, optic radiations, dorsal visual stream (parietal white matter 1 cm dorsal to the optic radiations), and hippocampi by using previously described methods.[35] These regions of interest were placed in the anatomic locations on the echo-planar T2-weighted images without knowledge of the locations of injury as determined by the T1-weighted and T2-weighted images or the D_{av} maps (Fig 1). In addition, D_{av} and FA maps were generated and were manually interrogated by the same 2 pediatric neuroradiologists with experience in neonatal brain imaging for areas of abnormal diffusivity. Average diffusivity and FA were assessed manually in most patients by placing a 1-mL circular region of interest over regions that appeared subjectively abnormal while recording the lowest value displayed in the region. The reason for this extra step was that the regions measured by standard anatomic voxel placements (discussed above and illustrated in Fig 1) did not always include sites of maximal abnormality. As with the spin-echo images, consensus was reached on all findings and agreement was high, with kappa of 0.9.

The T1-weighted images were used to guide the single-voxel MR spectroscopy volume selection, which was performed by using the point-resolved spectroscopic sequence (PRESS) technique to acquire the MR spectra from approximately 5.5 cm^3 of tissue for both regions. The spectrum for each location was acquired by using the GE PROBE (PROton Brain Examination) sequence in under 5 minutes with a TR = 2s, TE = 288ms, and 128 acquisitions. The MR spectroscopy timings and voxel localization were chosen to maximize the detection of lactate and to minimize the spectral contamination from extracranial adipose tissues. The 2 spectra were obtained with the same parameters and voxel size centered on the deep gray matter and then in the watershed region of the frontal white matter. Following acquisition the MR spectroscopy data were transferred off-line and analyzed on a computer workstation by using software developed in house for spectral quantification. Both a neuroradiologist and a basic scientist with extensive experience in MR spectroscopy analyzed all of the spectra. The MR spectroscopy data were Fourier transformed and baseline fitted, and the peak areas were integrated for the choline, creatine, *N*-acetylaspartate (NAA), and lactate resonances. Peak area ratios of lactate/choline, lactate/NAA, and NAA/choline were calculated for each voxel. In 2 patients, data were corrupted and some ratios could not be calculated. These ratios were marked in the data tables as missing data (MD).

For the MR spectroscopic imaging (MRSI), the PRESS technique was used to excite a selected region with further localization by 30

Table 1: Clinical, anatomic imaging, and diffusion (manual interrogation) data

Patient No.	Age at Scan	Clinical Background	T1-weighted images	T2-weighted images	Diffusion Images (D_{av}, mm^2/s)
153a	2 d (25.5 h)	Placental abruption, deep fetal decelerations and poor variability. Emergent C-section. Seizure at 8 hours, required 3 drugs	Slight hyperintensity in basal ganglia and at the depths of several cortical sulci. Absent hyperintensity in PLIC	Diffuse hyperintensity in white matter, basal ganglia	Reduced diffusivity in lateral thalami (0.70), posterior limbs of internal capsules (0.75)
153b	6 d (124 h)		Hyperintensity in dorsal brain stem, posterolateral putamina, lateral thalami	Slight hypointensity in posterolateral putamina and lateral thalami	Reduced diffusivity in posterior thalami (0.80), splenium of corpus callosum (0.80), and left more than right hemispheric white matter
154a	2 d (48 h)	Tight nuchal cord, variable decelerations. Multifocal seizures at 10 hours, treated with 4 drugs. Negative blood and CSF cultures and PCR	Normal	Blurring of cortex and white matter in anterior and posterior watershed zones	Reduced diffusivity in bilateral posterior thalami, anterior and posterior watershed cortex, and subcortical white matter
154b	4 d (91 h)		Normal	Blurring of cortex and white matter in anterior and posterior watershed zones	Reduced diffusion in posterior watershed cortex and white matter Slight persistent reduced diffusion in anterior watershed cortex Minimal persistent reduced diffusion in posterior thalami
155a	1 d (20 h)	Oligohydramnios, thick meconium, birth depression. Seizure on day of life 2, stopped with phenobarbital. Negative blood cultures	Normal PLIC present	Hyperintensity in white matter and thalami	Reduced diffusivity in watershed white matter
155b	6 d (124 h)		Normal PLIC present	Subtle gray-to-white blurring in posterior watershed cortex. Increased T2 in white matter and thalami	Reduced diffusivity in watershed white matter
155c	8 d (170 h)		Hyperintensity in watershed cortex	Hyperintensity in watershed cortex, posterior more than anterior	Normal
162a	2 d (46 h)	Maternal hypotension after epidural placement, fetal decelerations, C-sections, thick meconium. Seizures at 8 hours, treated with phenobarbital. Mom had history of herpes, but no lesions at labor, and PCR was negative for viruses in CSF	Slight hyperintensity in VLT, posterior putamen Faint hyperintensity in PLIC	Normal	Reduced diffusivity in left frontal subcortical white matter (0.50) and cortex, greater than right. Reduced diffusivity in VLT, left more than right (0.60–0.65)
162b	7 d (146 h)		Hyperintensity in left more than right frontal cortex, left GP	Normal	Reduced diffusivity in VLTs only (0.70–0.75)
163a	1 d (22 h)	Seizures in utero 3 days before birth. Crash C-section due to flat fetal heart rate. Infant seizing at delivery, nuchal cord1. PCR of CSF was negative	Hyperintensity in GP, putamen, caudate, VLT Absent hyperintensity in PLIC	Hyperintensity in most of cerebral cortex	Reduced diffusivity in VLTs (0.40), putamina (0.60), PLIC (0.55), subcortical white matter (0.70–0.75), dorsal BS (0.45–0.50)

163b	3 d (64 h)		Hyperintensity in GP, putamen, caudate, VLT, dorsal BS Absent T1 in PLIC	Hypointensity in dorsal BS, VLT, lateral putamen Long T2 in remainder of thalamus, much of cortex	Reduced diffusivity in hippocampi (0.45), subcortical white matter (0.45–0.50), basal ganglia (0.45), thalami (0.35), cerebellar vermis (0.50)
167a	1 d (19 h)	Pre-eclampsia, failed home labor, thick meconium, variable decelerations, crash C-section. After birth, persistent pulmonary hypertension, hypoglycemia, acute tubular necrosis. Blood cultures negative	Increased T1 in VLT Normal PLIC	Normal	Tiny area of reduced diffusivity in VLTs (0.85) Focal infarct left frontal lobe
167b	4 d (88 h)		Normal	Slight T2 prolongation in cortical infarcts	Small amount of reduced diffusivity in VLTs (0.60) and CSTs (0.70). Two focal infarcts, left frontal and left occipital
170a	2 d (34 h)	Uterine rupture, deep decelerations. Seizures at 9 hours. Blood cultures negative	Hypointensity in thalami Normal PLIC	Hyperintensity in thalami, basal ganglia	Reduced diffusivity in lateral thalami (0.55), CSTs (0.65), posterior BS (0.65–0.70)
170b	3 d (61 h)		Hypointensity in basal ganglia Hyperintensity not seen in PLIC	Hyperintensity in thalami, basal ganglia	Reduced diffusivity in putamen more than caudate, anterior and lateral thalami (0.40), CSTs (0.45–0.50), subthalamic nuclei, dorsal BS (0.50)
178a	1 d (16 h)	Maternal septic shock. Fetal tachycardia and abnormal fetal tracing. Thick meconium; no spontaneous activity or respirations at birth. Apgars 0, 0, 1 at 1, 5, and 10 minutes. Transient hepatic and renal dysfunction. Seizures before first MR image. Blood and CSF cultures of infant were negative	Hyperintensity in caudate, GP, putamen Normal PLIC	Hypointensity in VLT Blurring of perirolandic cortex	Reduced diffusivity in VLTs (0.65), CSTs (1.0)
178b	4 d (83 h)		Hyperintensity in VLT, GP, posterior putamen, posterior insula Hyperintensity not seen in PLIC	Normal	Reduced diffusivity in posterior putamina (0.55), VLTs (0.50), CSTs (0.70–0.75), CC (0.75), subcortical white matter (0.60)
178c	7 d (178 h)		Globular hyperintensity in VLTs, GP–putamen junction, posterolateral putamen. Hyperintensity not seen in PLIC	Heterogeneous basal nuclei. T2 prolongation in cerebral white matter	Reduced diffusivity in posterior putamen (0.70). Minimally reduced in VLTs (0.90), CSTs (1.0).
193a	2 d (34 h)	Home delivery complicated by LGA infant and shoulder dystocia. After prolonged delivery, infant was cyanotic, limp. Infant was given CPR for 40 minutes before spontaneous respirations. Seizures at about 5 hours, treated with phenobarbital	Hyperintensity in VLTs, GPs, putamina, caudates, most of cerebral cortex. Normal PLIC	Hyperintensity of BG, thalami. Blurring of perirolandic cortex	Reduced diffusivity in VLTs (0.45–0.50), CSTs (0.60)
193b	7 d (148 h)		Hyperintensity in VLTs, GPs, putamina, caudates, posterior insular cortex, perirolandic cortex, calcarine cortex Hyperintensity not seen in PLIC	Normal	Reduced diffusivity in cingulum (0.65), corpus callosum (0.60), fronto-occipital fasciculus (0.95), optic radiations (0.90), uncinate fasciculus (0.85)
195a	2 d (44 h)	Jittery baby. Mild hypoglycemia. Low normal ABG pH	Normal. Hyperintensity present in PLIC	Normal	Normal
195b	19 d (330 h)		Focus of hyperintensity in right frontal periventricular white matter	Normal	Normal

Note:—D_{av} indicates average diffusivity; PLIC, posterior limb of internal capsule; ABG, arterial blood gas; VLT, ventrolateral thalamus; CST, corticospinal tract; GP, globus pallidus; CC, corpus callosum; LGA, large for gestational age; CPR, cardiopulmonary resuscitation; CSF, cerebrospinal fluid; BS, brain stem; PCR, polymerase chain reaction.

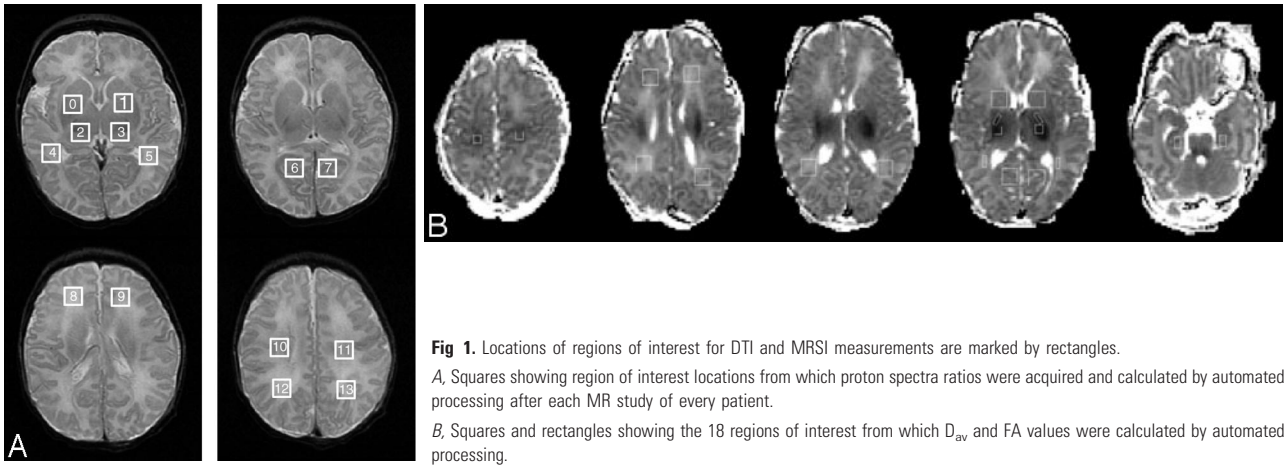

Fig 1. Locations of regions of interest for DTI and MRSI measurements are marked by rectangles.

A, Squares showing region of interest locations from which proton spectra ratios were acquired and calculated by automated processing after each MR study of every patient.

B, Squares and rectangles showing the 18 regions of interest from which D_{av} and FA values were calculated by automated processing.

chemical shift imaging (CSI) as described elsewhere.[37] Optimized shaped pulses designed by using the Shinnar-Le Roux algorithm allowed improved water suppression and section selection profile in comparison with conventional pulses.[38] The PRESS selected volume included a region of approximately 60–200 mL, which encompassed most the neonate brains while excluding the spatial inclusion of subcutaneous lipids. Phase-encoding in the PRESS-CSI sequence was used to obtain $8 \times 8 \times 8$, $12 \times 12 \times 8$, or $16 \times 8 \times 8$ 3D spectral arrays with a nominal spatial resolution of 1 mL Following a 2–3-minute prescan procedure including autoshimming, 3D PRESS MRSI (with very selective saturation [VSS] pulses to provide improved coverage and excitation profiles) was acquired in a 17- or 19-minute acquisition. The MR images and raw MRSI data were transferred off-line to a Sun UltraSparc workstation (Sun Microsystems, Mountain View, Calif) for analysis by using software developed at our institution for 3D MRSI processing. Spectral processing included 4D Fourier transformations, automatic frequency and phase adjustments, baseline fitting, and peak integration. This software also provides postprocessing alignment of the spatial center of the spectral arrays. This was used to center the MRSI data to the PRESS selected regions and to position 1-cm^3 spectral voxels in specific anatomic locations as defined from the MR images by using a custom-designed region of interest tool. The region of interest tool and MRSI display tool were written in the Interactive Display Language (IDL; Research Systems, Inc., Boulder, Colo). To define voxels that were within the selected regions (and not in the saturation bands surrounding the selected volume) and have adequate signal intensity-to-noise (SNR peak height/noise height), the noise and SNR were calculated for each voxel and metabolite. To avoid spuriously large metabolite ratios, ratios are reported only for voxels with a choline SNR >5.

To assess the MR spectra in various anatomic locations in the brain, spectral voxels were retrospectively centered in the following regions bilaterally: (1) basal ganglia (BG), (2) thalamus (TH), (3) optic radiations (OR), (4) corticospinal tracts (CS), (5) frontal white matter (FWM), (6) calcarine gray matter (CGM), and (7) parietal white matter (PWM). The locations are shown for a representative case in Fig 1. These 7 voxel locations were chosen for several reasons: they include both more mature (deep gray matter) and less mature (frontal white matter) portions of the brain; they involve areas that are important in motor (corticospinal tracts, basal ganglia), visual (calcarine cortex, thalamus), and cognitive (frontal and parietal white matter) function; and they include the regions commonly injured in neonatal brain injury (deep gray nuclei, frontal intervascular boundary zones). Three regions (posterior limb of internal capsule, dorsal visual stream, and hippocampi) in which diffusivity data were assessed could not be adequately assessed by MRSI because of the very small size preventing adequate SNR (posterior limb of internal capsule) or because the regions were outside of the PRESS selected volume. Several voxels from various scattered regions of interest were not assessed in many of the patients because of similar difficulties in SNR or location of the PRESS selected volume.

Statistical Analysis

Graphic and descriptive statistics were used to present the MR data. The limited sample size and the large number of predictor variables precluded a meaningful statistical analysis of the imaging characteristics and the affected children with regard to outcome and time of study.

Results

The initial study was performed on day 1 (within 24 hours of birth) in 4 neonates and on day 2 (between 24 and 48 hours after birth) in 6 neonates. The second scan was performed on day 3 (61–64 hours after birth) in 2 neonates, on day 4 (83–91 hours after birth) in 3 neonates, on day 6 in 2, on day 7 in 2, and on day 14 in one. (The patient studied on day 14 was discharged to home and returned for the follow-up scan as an outpatient. The long interval between the first and second scan was caused by scheduling difficulties for both the family and the hospital). The third scan was performed on day 8 in both neonates (Table 1). D_{av} values from the voxels sampled by automated processing (Fig 1) are shown in Table 2. Metabolite ratios from the single voxel proton spectroscopy are shown in Table 3. The metabolite ratios from the voxels sampled by automated processing of the MRSI are not shown because the enormous volume of data (8 ratios per voxel times 14 voxels) was too much to display. Similarly, all of the calculated values from the diffusion data are too numerous to display; because analysis of these anisotropy and individual eigenvalues were not revealing but the D_{av} values were, only the D_{av} values are displayed in the Table.

Spin-Echo and Diffusion Studies

Evaluation of Studies by Days after Birth. The visually apparent MR imaging findings changed considerably as the time after birth lengthened. Examinations performed on day 1 showed very subtle findings on the T1 and T2-weighted images (Table 1). One study was completely normal, whereas a

Table 2. Diffusion data from automated processing

Patient No.	Dav V0	Dav V1	Dav V2	Dav V3	Dav V4	Dav V5	Dav V6	Dav V7	Dav V8	Dav V9	Dav V10
153a	1274.24	1278.57	912.551	948.122	1481.61	1407.82	1176.6	1199.73	1344	1303.29	1497.69
153b	N/A	N/A	N/A	N/A	N/A	N/A	N/A	N/A	N/A	N/A	N/A
154a	1117.53	1111.89	946.773	937.83	1281.96	1350.27	1079.62	1109.05	1065.62	1097.97	1326.35
154b	1237.79	1199.41	1110.94	1077.08	1364.24	1348.91	1140.5	1206.36	1179.75	1300.34	1125.61
155a	1149.22	1183.5	997.95	1056.08	1236.5	1316.49	1154.74	1215.4	1198.18	1109.86	1538.64
155b	845.5	824.827	768.009	712.835	956.855	1009.75	849.545	842.436	857.864	866.35	958.491
155c	1287.58	1280.5	1157.1	1118.98	1428.45	1420.55	1222.6	1231.45	1553.6	1337.48	1691.56
162a	1093.49	1117.43	975.102	957.429	1231.08	1279.31	1108.83	1121.71	1032.18	1165.36	1292.57
162b	1210.61	1174.37	1008.33	1021.61	1335.98	1283.27	1207.29	1188.76	1231.41	1256.41	1553.59
163a	1029.65	1013.39	712.633	714.347	1334.59	1210.96	1092.9	1110.41	1302.2	1354.76	1824.82
163b	693.694	674.898	649.816	583	862.429	935.776	841.918	856.878	758.776	914.232	1002.63
167a	1239.98	1251.2	1026.67	977.107	1399.39	1307.88	1209.84	1218.98	1286.93	1329.55	1447.08
167b	1180.67	1166.73	1008.43	989.755	1290.06	1347.55	1197.23	1217.22	1168.47	1196.41	1282.24
170a	1195.67	1196.51	622.429	732.898	1378.24	1398.45	1277.43	1255	962.408	1049.69	1374.71
170b	981.286	942.5	601.122	603.959	1400.65	1484.71	1158.33	1112.96	1436.92	1424.49	1346.39
178a	1214.62	1231.98	987.5	906.667	1524.8	1545.3	1160.25	1274.14	1195.75	1249.19	1572.71
178b	1169.94	1149.71	1118.17	1194	1615.1	1515.7	1326.11	1245.22	1308.75	1246.69	1751.57
178c	1179.79	1180.63	1129.75	1128.58	1507	1515.9	1242.98	1199.29	1288.33	1333.08	1492.29
193a	1105.36	1135	582.5	702.583	1439.2	1357.8	1141.46	1126.59	1089.44	1066.25	1423.18
193b	1104.86	1049.86	822.75	783	1200.6	1181.5	1174.22	1296.2	1088.94	1078.33	1280.31
195a	1329.41	1295.59	1155.67	1217	1247.5	1369.8	1177.22	1196.14	1148.33	1172.12	1317.49
195b	1154.51	1192	956	1076.5	1340.7	1335.6	1123.96	1264.31	1094.5	1134.81	1330.12

Note:—Dav V indicates diffusivity in Voxel; N/A, data not available.

second showed only edema (T1 and T2 prolongation) in the basal ganglia or white matter. The third and fourth showed slight hyperintensity in the basal ganglia and at the depths of a few cortical sulci on T1-weighted images; both of these patients (163 and 178) had possible prenatal injury. (Clinical summaries are given in Table 1.) Calculated diffusivity images of these patients showed reduced diffusivity in the watershed regions of cortex (in one patient) or the ventrolateral deep gray nuclei or corticospinal tracts (3 patients); one with reduced diffusivity in the thalami also had reduced diffusion in a small cortical infarct. D_{av} values in the affected regions of these patients were reduced between 10% (D_{av} of ~0.85 mm^2/s in the thalami compared with normal values of about 0.950 mm^2/s) and 60% (0.40 mm^2/s in the thalami) (Tables 1 and 2); the one with the most significant reduction (Fig 2) in D_{av} had possible prenatal injury (patient 163).

Of the 6 patients studied initially on day 2, 3 studies showed T1 shortening (T1 hyperintensity) in the basal ganglia and thalami; one of these had normal T2-weighted images, whereas the other had diffuse T2 hyperintensity in the brain. All of these patients had reduced diffusivity in the lateral thalami and posterior limbs of the internal capsules; D_{av} values ranged from about 0.50 mm^2/s to 0.65 mm^2/s. One subject also had reduced diffusivity in the left greater than right frontal subcortical white matter; D_{av} values were markedly reduced to about 0.50 mm^2/s in the most affected location. The fourth patient initially studied on day 2 had T2 prolongation and blurring of the watershed cortex and underlying white matter (reduced diffusivity was seen in these areas, as well as in the posterior thalami), while the fifth had T1 and T2 prolongation (hypointensity on T1-weighted images, hyperintensity on the T2-weighted images) and reduced diffusivity in the basal ganglia, thalami, and dorsal brain stem. The sixth patient had normal T1 and T2-weighted images and normal brain diffusivity. Normal hyperintensity was seen in the posterior limb of the internal capsule in all patients studied on days 1 and 2, except 2 who were born at 36 and 37 weeks. On the diffusivity maps, D_{av} values from anatomic ROIs ranged from 0.60 to 0.90 mm^2/s, which is reduced about 10%–40%, in the basal ganglia and thalami, whereas it was reduced about 15% in the watershed region of the patient with watershed injury (Tables 1 and 2).

The 2 patients studied on day 3 had very different appearances on conventional imaging. Patient 163 (who had a presumed prenatal injury) had hyperintensity of the globi pallidi, putamina, caudates, ventrolateral thalami, and dorsal brain stem on T1-weighted images and a heterogeneous picture on T2-weighted images, with hypointensity in the dorsal brain stem, ventrolateral thalami, and posterior putamina but hyperintensity in the remainder of the thalami and most of the cerebral cortex. Extensively reduced diffusion was seen in the hippocampi, subcortical white matter, basal ganglia, thalami, and corticospinal tracts (D_{av} values were reduced 30%–40% throughout the brain in the standard regions of interest, and 60%–70% by manual interrogation) (Fig 2 and Tables 1 and 2). In patient 170, the conventional images continued to show T1 and T2 prolongation, whereas the D_{av} maps showed increasing spatial extent of the regions of reduced diffusivity and the values themselves decreased another 20% in the deep gray nuclei and dorsal brain stem compared with the study performed 27 hours earlier (Fig 3). The normal hyperintensity in the posterior limb of the internal capsule was absent in both; however, patient 163 was born at 37.5 weeks and the lack of hyperintensity may well have been the result of immaturity.

Three patients were studied on day 4. Patient 154 had a normal T1-weighted study and had blurring in the watershed regions on the T2-weighted images; reduced diffusion was present in the anterior and posterior watershed regions and in the posterior thalami. Patient 167 had a normal T1-weighted study and the T2-weighted images showed only slight hyper-

Table 3: Metabolite ratios from the single voxel proton spectroscopy

Patient No.	Age at Study	Lac/Ch (BG)	Lac/NAA (BG)	NAA/Ch (BG)	Cr/NAA (BG)	Cr/Ch (BG)	Lac/Ch (W/M)	Lac/NAA (WM)	NAA/Ch (WM)	Cr/NAA (WM)
153a	2 d	0.58	1.26	0.46	0.88	0.41	MD	MD	MD	MD
153b	6 d	0.65	1.89	0.34	0.97	0.33	MD	MD	MD	MD
154a	2 d	0.14	0.20	0.72	0.69	0.49	0.47	0.67	0.71	0.51
154b	4 d	0.19	0.22	0.83	0.72	0.60	0.30	0.56	0.53	0.78
155a	1 d	0.17	0.22	0.79	0.60	0.47	0.39	0.63	0.62	0.62
155b	6 d	0.12	0.20	0.62	0.80	0.50	0.23	0.40	0.59	0.61
155c	8 d	0.07	0.10	0.72	0.80	0.57	0.12	0.25	0.47	0.73
162a	2 d	0.09	0.12	0.75	0.72	0.54	0.39	0.63	0.62	0.58
162b	7 d	0.04	0.06	0.68	0.55	0.37	0.11	0.19	0.56	0.38
162b	7 d	0.04	0.06	0.68	0.55	0.37	0.11	0.19	0.56	0.38
163a	1 d	0.99	1.73	0.57	0.95	0.54	1.11	1.94	0.57	0.86
163b	3 d	1.06	2.81	0.38	1.09	0.41	1.13	2.78	0.41	0.90
167a	1 d	0.16	0.17	0.93	0.52	0.49	0.13	0.19	0.69	0.61
167b	4 d	0.15	0.21	0.72	0.64	0.46	0.15	0.20	0.74	0.52
170a	2 d	MD	MD	MD	MD	MD	MD	MD	MD	MD
170b	3 d	MD	MD	MD	MD	MD	MD	MD	MD	MD
178a	1 d	0.15	0.25	0.60	0.59	0.35	0.28	0.34	0.80	0.48
178b	4 d	0.48	0.90	0.54	0.86	0.46	0.34	0.49	0.69	0.60
178c	8 d	0.23	0.35	0.66	0.85	0.56	0.20	0.37	0.55	0.66
193a	2 d	0.38	0.40	0.95	0.60	0.57	0.40	0.51	0.77	0.43
193b	7 d	0.43	1.17	0.37	0.86	0.32	0.49	1.38	0.35	0.69
195a	2 d	0.04	0.50	0.75	0.57	0.43	0.01	0.02	0.64	0.62
195b	14 d	0.00	0.00	0.91	0.54	0.49	0.01	0.02	0.87	0.37

Note:—Ch indicates choline; NAA, *N*-acetylaspartate; MD, missing data.

intensity of the cortex at the site of 2 focal infarcts; our standard regions of interest of the D_{av} maps showed minimally reduced diffusivity of the ventrolateral thalami and posterior limbs of the internal capsules and significantly reduced diffusion at the sites of the infarcts. Manual interrogation of the D_{av} maps, however, showed more significantly reduced diffusivity, with values reduced about 30% in the ventrolateral thalamus, putamina, and dorsal brain stem. Patient 178 had marked diffuse T1 shortening in the lateral thalami, globi pallidi, posterior putamina, and posterior insular cortices, absence of hyperintensity of the posterior limb of the internal capsule, and extensive reduced diffusivity in the lateral thalami, posterior putamina, and subcortical white matter (Fig 4). D_{av} values in patient 178 were 0.50 mm^2/s in the ventrolateral thalamus and dorsal midbrain, 0.55–0.60 mm^2/s in the posterior putamen, 0.70–0.75 mm^2/s in the corticospinal tracts of the centrum semiovale, and 1.20–1.30 mm^2/s in the central white matter of the centrum. No scans were performed on day 5.

Of the scans performed on day 6, patient 155 had only subtle diffuse edema, blurring of the cortex in the posterior watershed cortex on T2-weighted images and reduced diffusivity throughout the cerebral hemispheres. In the deep gray matter, diffusivity values were down 10%–30%, whereas values in the hemispheric white matter were 30%–40% below normal. Patient 153 had T1 and T2 shortening in the dorsal brain stem, posterolateral putamina, and lateral thalami with reduced diffusivity (by about 10%–20%) in the posterior thalami, corpus callosum, and extensively through the white matter of the cerebral hemispheres.

Both studies performed on day 7 showed extensive diffuse T1 shortening in the affected areas, in the frontal cortex in patient 162 and in the basal ganglia, insula, perirolandic cortex and the calcarine cortex in patient 193. D_{av} maps showed reduced diffusivity only in the ventrolateral thalami in the former (with D_{av} values about 20% below normal on the region of interest and about 30% below normal on the manual assessments) but showed reduced diffusivity also in the cingulum (50% of normal), corpus callosum (60% of normal), optic radiations (70% of normal), and fronto-occipital fasciculus (70% of normal) in the latter (Fig 5). These abnormal D_{av} values in the white matter were not detected by our standard region of interest placements (Tables 1 and 2).

On day 8, patient 155 (with watershed injury) showed T1 shortening and T2 prolongation in the watershed cortex, with the posterior regions affected more severely than the anterior regions; D_{av} values had normalized. The scan of patient 178 showed a transformation from diffuse, hazy T1 shortening in the basal ganglia to multifocal, globular T1 shortening at the ventrolateral thalami, posterolateral putamina, and the globus pallidus-putamen junctions, heterogeneity of the basal ganglia on T2-weighted images, and reduced diffusion largely localized to the posterior putamina (Fig 4). Manual interrogation of the diffusivity maps revealed that D_{av} values of the thalami, corpus callosum, and central white matter had returned to normal, while those of the posterior putamina remained low by about 25% (Table 1).

On day 14, patient 195 had a small new focus of T1 shortening in the right frontal white matter, normal T2-weighted images, and normal D_{av} values.

Evaluation of Sequential Studies. Looking at the sequential studies patient by patient, several patterns become clear, whereas others are suggested. All patients either developed new areas of T1 shortening or developed more extensive T1 shortening on their second scan as compared with their first scan. In patients with the watershed pattern of injury, this was manifested as T1 shortening in the depths of sulci in the watershed regions, whereas the patients with basal ganglia pattern of injury manifested increasing T1 shortening in the basal

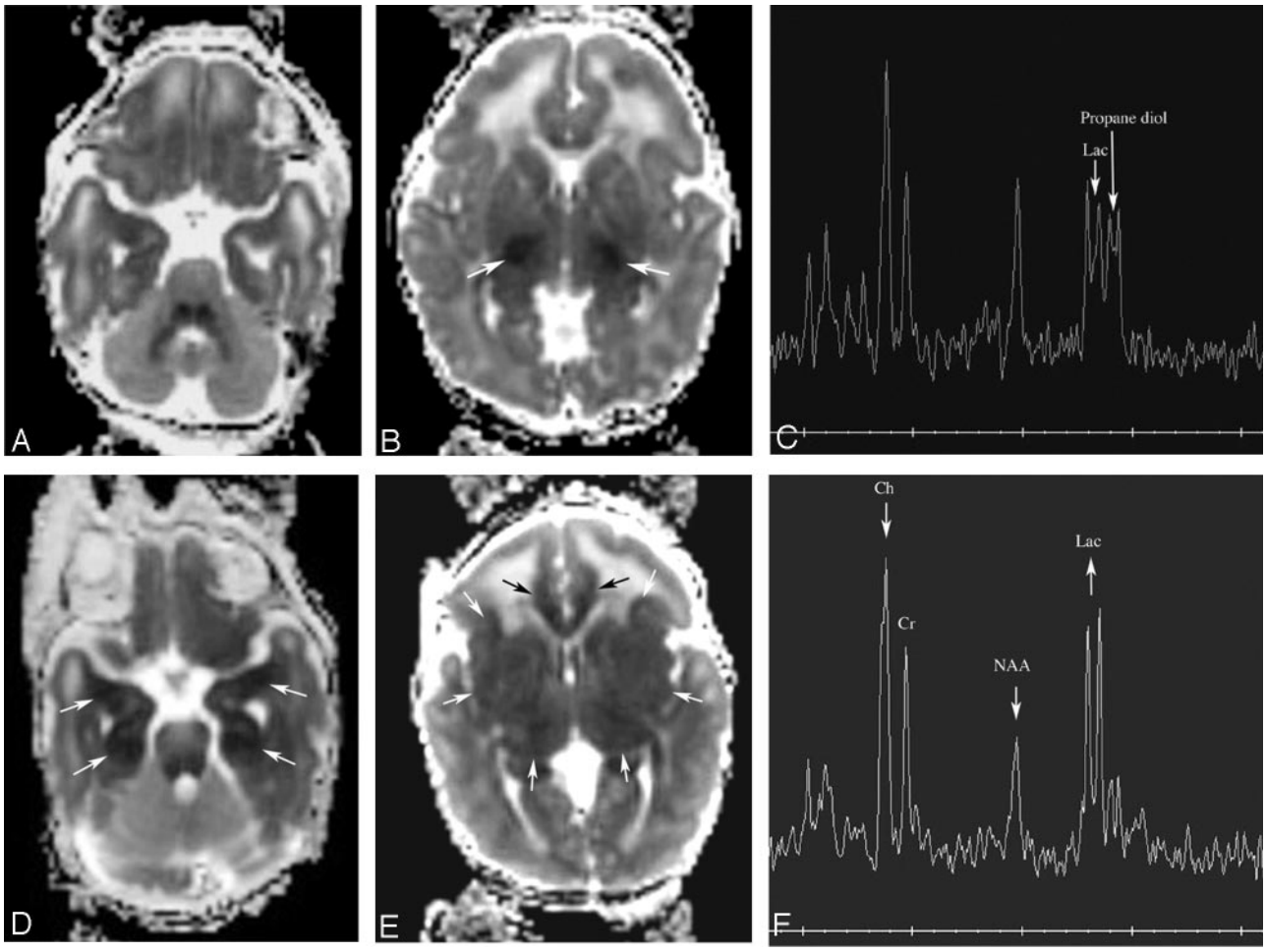

Fig 2. Patient 163. Increasing abnormality from day 1 to day 3.

A and *B,* Axial D_{av} maps at age 22 hours (day 1) show reduced diffusion in the ventrolateral thalami (*arrows*) and normal-appearing mesial temporal lobes in the region of the uncus.

C, Proton MR spectroscopy from left thalamus at 22 hours shows elevated lactate peak (Lac) and normal appearing NAA peak. The peak upfield from lactate is propane diol (ethylene glycol), which is administered as the base for antiseizure medications.

D and *E,* Axial D_{av} maps at age 64 hours (day 3) show more extensive reduced diffusivity. The mesial temporal lobes (*D, white arrows*) show reduced Dav, as do the cingula (*E, black arrows*) and the entire basal ganglia-thalami-insular region (*E, white arrows*).

F, Proton MR spectroscopy from left thalamus at 64 hours shows interval increase in lactate and decrease in NAA and choline (Ch) compared with creatine (Cr).

ganglia, thalami, and perirolandic cortex. By the third study in patient 178 (on day 8), the character of the T1 shortening changed from a diffuse hyperintensity to a more focal, globular hyperintensity that was largely concentrated in the ventrolateral thalamus, posterior putamen and at the globus pallidus-putamen junction (Fig 4). The third study of patient 155, who had primarily watershed injury, did not significantly change from the second study.

The abnormalities seen on T2-weighted images were few and did not significantly evolve during the sequential studies, with the exception of the 2 patients who had cortical infarcts (both of these become more conspicuous on the second scan compared with the first) and patient 178 with extensive deep gray matter and cortical injury in whom the third study (178c) showed areas of hypointensity developing in the ventrolateral thalami and posterior putamina, resulting in a heterogeneous appearance to the brain.

The abnormalities of diffusivity evolved the most. The initial studies, performed within 48 hours of birth, typically had very localized diffusion abnormalities, with varying reduction of D_{av} values. In the neonates with the basal ganglia pattern, reduced diffusivity was most marked in the ventrolateral thalami or the ventrolateral thalami and the posterior limb of the internal capsule with D_{av} values ranging from 5% to 30% less than normal in the regional regions of interest and from 10% to 60% less than normal on the manual assessments of the structures; in severe cases, the dorsal brain stem was also involved. If the second study was performed on days 3–5, the area of reduced diffusion in the thalami had grown and reduced diffusion almost invariably involved the basal ganglia and corticospinal tracts; although the D_{av} values in the thalami continued to go down (by another 10%–20%) until day 4–5, the D_{av} values in the adjacent areas decreased much more (by 20%–30%) (Tables 1 and 2). This increase in area of abnormal diffusivity was also seen when damage was primarily in the intervascular boundary zones (Fig 6), in addition to those with the deep gray matter pattern of injury. In addition, in 3 patients with the deep gray matter pattern the subcortical white matter developed reduced diffusion (Figs 5). Patient 193, who had a follow-up scan at age 7 days, showed normalization of

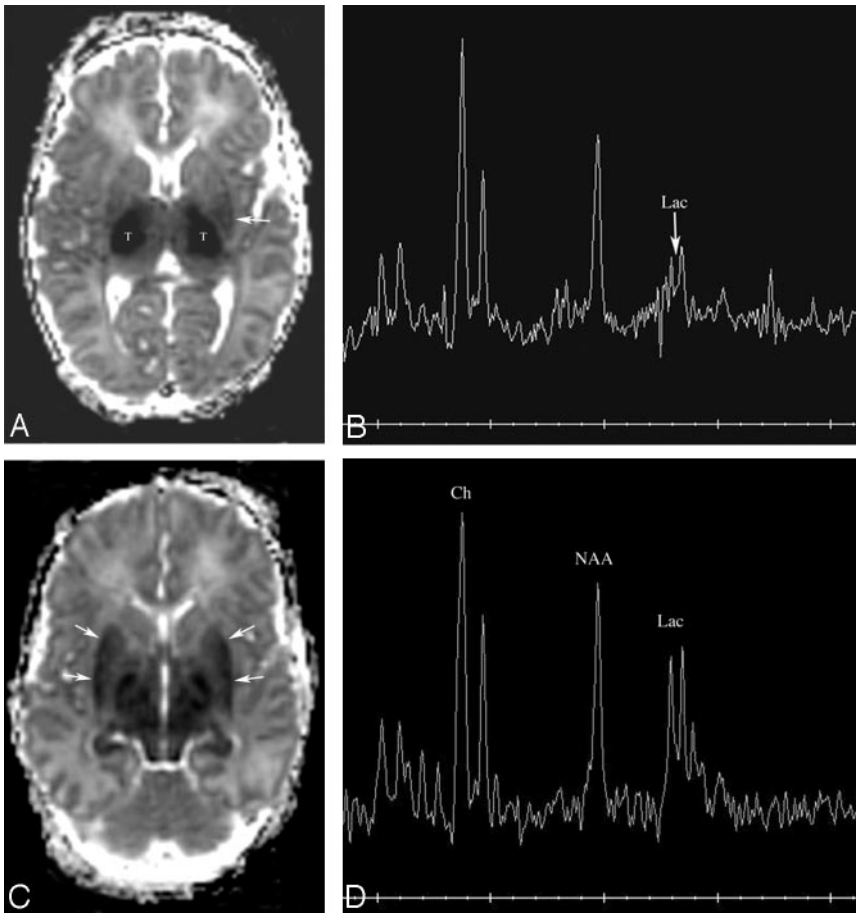

Fig 3. Patient 170. Increasing abnormality from day 2 to day 3.

A, Axial D_{av} map at age 34 hours shows extensive reduced diffusion in the lateral thalami (T) and, to a lesser extent, in the posterior left putamen (*white arrow*).

B, Proton MR spectroscopy from the left thalamus at 34 hours is most remarkable for a moderate lactate peak (*arrow*).

C, Axial D_{av} map at age 61 hours shows that extensive reduced diffusivity has developed within the putamina (*arrows*).

D, Proton MR spectroscopy from the left thalamus at 61 hours shows a marked increase in lactate compared with NAA and choline.

diffusivity in the ventrolateral thalamus and corticospinal tracts but was found to have new areas of reduced diffusivity (on the D_{av} maps) in the cingulum, corpus callosum, optic radiations, and fronto-occipital fasciculus (Fig 5). Patient 162, also followed at age 6 days, showed normalization of reduced diffusion in the frontal cortex and subcortical white matter. In patient 178, who had a third scan at age 8 days, the diffusivity returned to normal in the corticospinal tracts and much of the thalami and putamina; reduced diffusion was limited to the posterior putamina, a tiny area in the posterolateral thalami, the corpus callosum, and the corticospinal tracts (Fig 4). In patient 195, who had a follow-up scan at 14 days, the D_{av} map and D_{av} values had returned to completely normal.

MR Spectroscopy

Unfortunately, in a number of patients some of the regions of interest for some of the white matter areas of interest were located outside of the PRESS selected volume on the 3D acquisitions, and, as a result, no metabolite ratios could be obtained for those regions. In addition, some white matter voxels had inadequate SNR (choline SNR peak height/noise height <5) and were therefore excluded. Nonetheless, good data were obtained for most of the single voxel spectra, for all of the basal ganglia, thalami, and calcarine regions on the 3D acquisitions, and for a large most of the white matter regions on the 3D acquisitions, which allowed a detailed analysis of the evolution of metabolite ratios. Data from the single voxel spectra are displayed in Table 3.

NAA/Ch generally went down after injury in the injured region, from the time of the first scan until the second scan. It then went back up again on the third study in the 2 patients with 3 scans. NAA/Ch also went up from day 2 to 14 in patient 195, who had a mild injury. These changes likely reflect both temporary and permanent changes in the quantity of NAA, which is known to decrease after injury, though we cannot be certain that there is not a transient rise in choline after injury (with mobilization of membrane fragments) contributing to the decreasing ratio. After the acute injury, one would expect choline to decrease again and to continue to decrease as part of its normal developmental incorporation into macromolecules.[39]

Cr/NAA went up from first to second scan in every patient except patient 162, who was the patient in whom the ADC returned to normal by day 6. The ratio minimally decreased on the third scan in both patients. No recognizable pattern was discerned in the Cr/Ch ratios.

Lac/NAA in the basal ganglia and thalami always increased when the first MR spectroscopy was performed on day 1 and the second on day 2, 3, or 4 (4 patients, Figs 2–4). In patient 193, it increased between day 2 and day 7 (Fig 5). Lac/NAA in the watershed voxels was more variable, increasing from day 1 to day 3, staying stable or increasing from day 1 to day 4, decreasing from day 1 to day 5 and day 2 to day 4 (Fig 6), but increasing from day 2 to day 7 and from day 2 to day 14. Of interest, Lac/NAA in patient 163 decreased slightly in the white matter voxels from day 1 to day 3, whereas Lac/NAA was markedly increasing in the basal ganglia and thalami. In both patients with a third study, Lac/NAA decreased in the thalami, basal ganglia, calcarine cortex, and watershed voxels, though the ratio dropped considerably less in the watershed voxels than in the deep gray nuclei.

Discussion

Many reports have described the MR imaging findings, metabolite ratios, and diffusion characteristics in encephalopathic neonates.[1-23] Other than the paper of McKinstry et al,[21] these works have not addressed the evolution of these MR parameters in individual patients who were studied sequentially. The sequential changes after prenatal, perinatal, or neo-

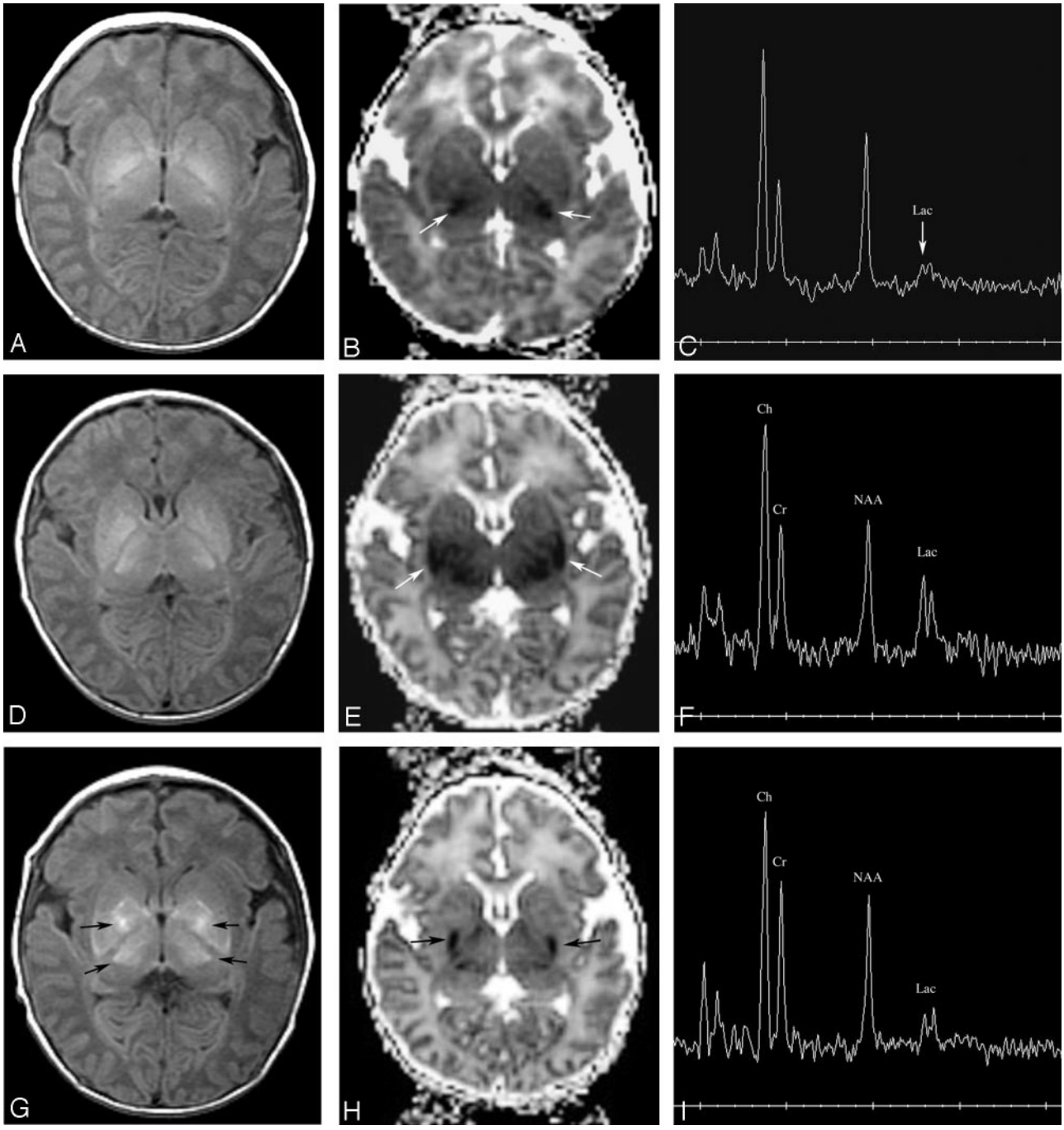

Fig 4. Patient 178. Evolution of T1, diffusivity, and metabolites over 3 scans during 8 days. *A–C* were performed at day 1 (16 hours), *D–F* were performed at 4 days (84 hours), and *G–I* were performed at 8 days (178 hours).

A, Axial T1-weighted image at age 16 hours is normal.

B, Axial D_{av} map at age 16 hours shows a small amount of reduced diffusivity on the ventrolateral thalami (*arrows*). Measurements showed a reduction in D_{av} of about 10%.

C, Proton MR spectroscopy from the right thalamus at age 16 hours shows minimal elevation of lactate (Lac), but is otherwise normal.

D, Axial T1-weighted image at 84 hours shows that the normal hyperintensity in the posterior limb of the internal capsule is no longer seen. Abnormal hyperintensity is seen in the ventrolateral thalami and posterior putamina.

E, Axial D_{av} map at 84 hours shows that reduced diffusivity is now present in the posterior putamina (*arrows*). Measurements of D_{av} showed significant reduction since day 1, with values now 50%–60% or normal (40%–50% reduced) in the thalami and putamina, and dorsal brain stem. Lesser reductions of about 25% were found in the cerebral hemispheric white matter.

F, Proton MR spectroscopy from the right thalamus at 84 hours shows an increase in lactate (Lac) and relative reduction of choline and NAA compared with the first study.

G, Axial T1-weighted image at 8 days shows that the T1 shortening is becoming less diffuse and more globular (*arrows*), with the globular regions being located in the globi pallidi, ventrolateral thalami, and at the junction of the anterior globi pallidi and putamina.

H, Axial D_{av} map at 84 hours shows that reduced diffusivity is now almost exclusively seen in the posterior putamina (*arrows*) with the thalamic abnormality nearly completely gone. Measurements showed that the D_{av} values of the putamina were still about 30% below normal, but those in the thalami had normalized.

I, Proton MR spectroscopy from the right thalamus at 8 days shows that the lactate peak has gotten significantly smaller. Note that the NAA and choline peaks have continued to decrease in size compared with the creatine peak.

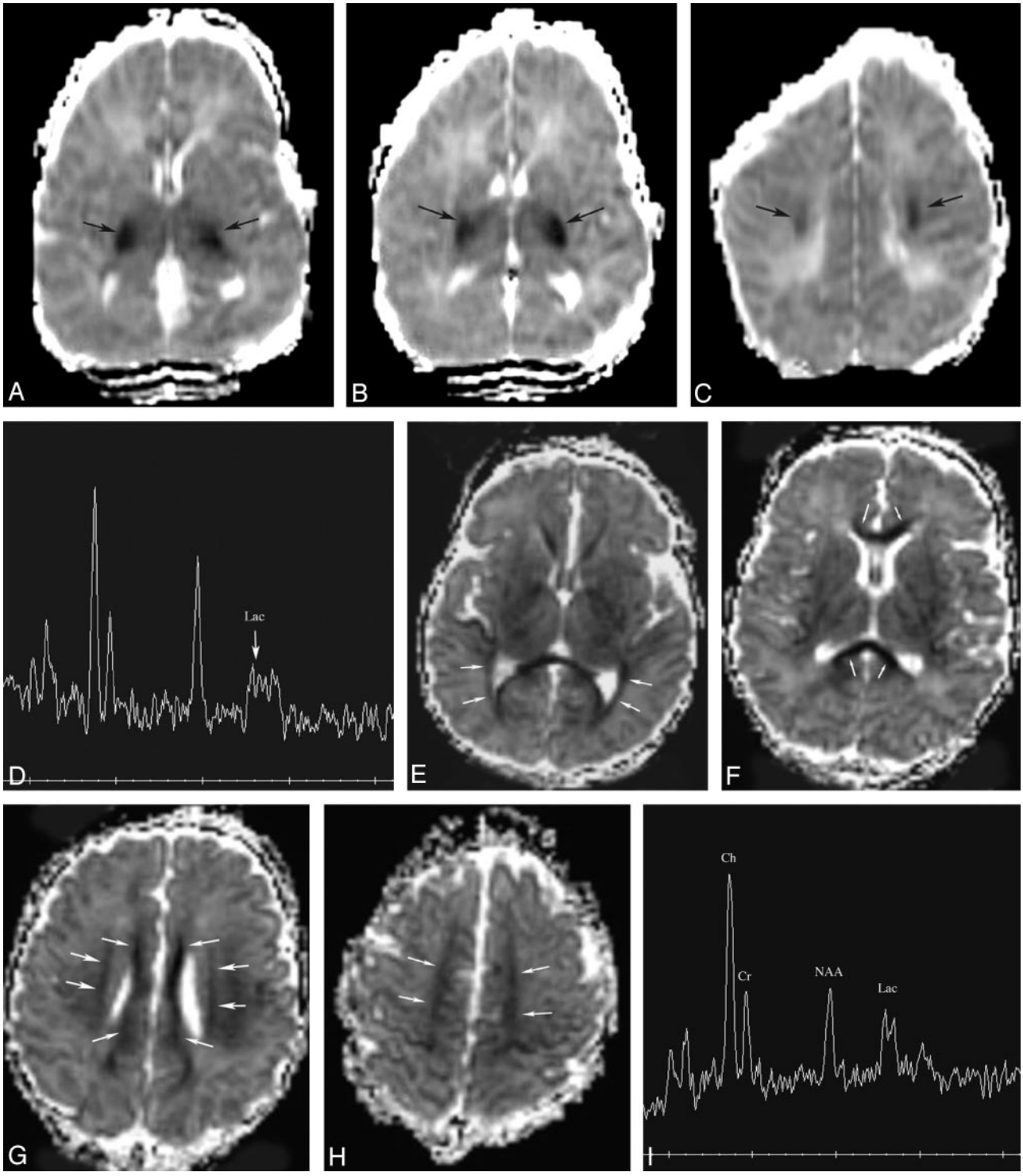

Fig 5. Patient 193. New involvement of white matter pathways on second study. Studies performed at day 2 and day 7.

A–C, Axial D_{av} maps at 34 hours show reduced diffusivity (D_{av} reduced by about 50%, *black arrows*) in the ventrolateral thalami, posterior limbs of internal capsules, and corticospinal tracts in centrum semiovale. No other areas of reduced diffusivity are identified.

D, Proton MR spectroscopy from the left basal ganglia at 34 hours shows mild lactate (Lac) elevation.

E–H, Axial D_{av} maps at 148 hours show that diffusivity in the deep gray nuclei has normalized (values were within 5% of normal); however, new areas of reduced diffusivity are seen in what are believed to be the optic radiations (*E, medium white arrows*), corpus callosum (*F, small white arrows; G, smaller white arrows*), cingulum (*H, medium white arrows*), and superior longitudinal fasciculus (*G, larger arrows*).

I, Proton MR spectroscopy from left basal ganglia at 148 hours shows that lactate (Lac) has increased in comparison with NAA, choline, and creatine. NAA is the most reduced metabolite.

natal injury are of importance in that these studies are typically performed at variable times after birth, depending on the severity of the injury, the stability of the neonate, and the availability of scanner time. Various parameters, such as T1 and T2 characteristics,[11-13] metabolite ratios,[1,4,11,40] and diffusivity[14,21] seem to vary with the time after injury but the timing of

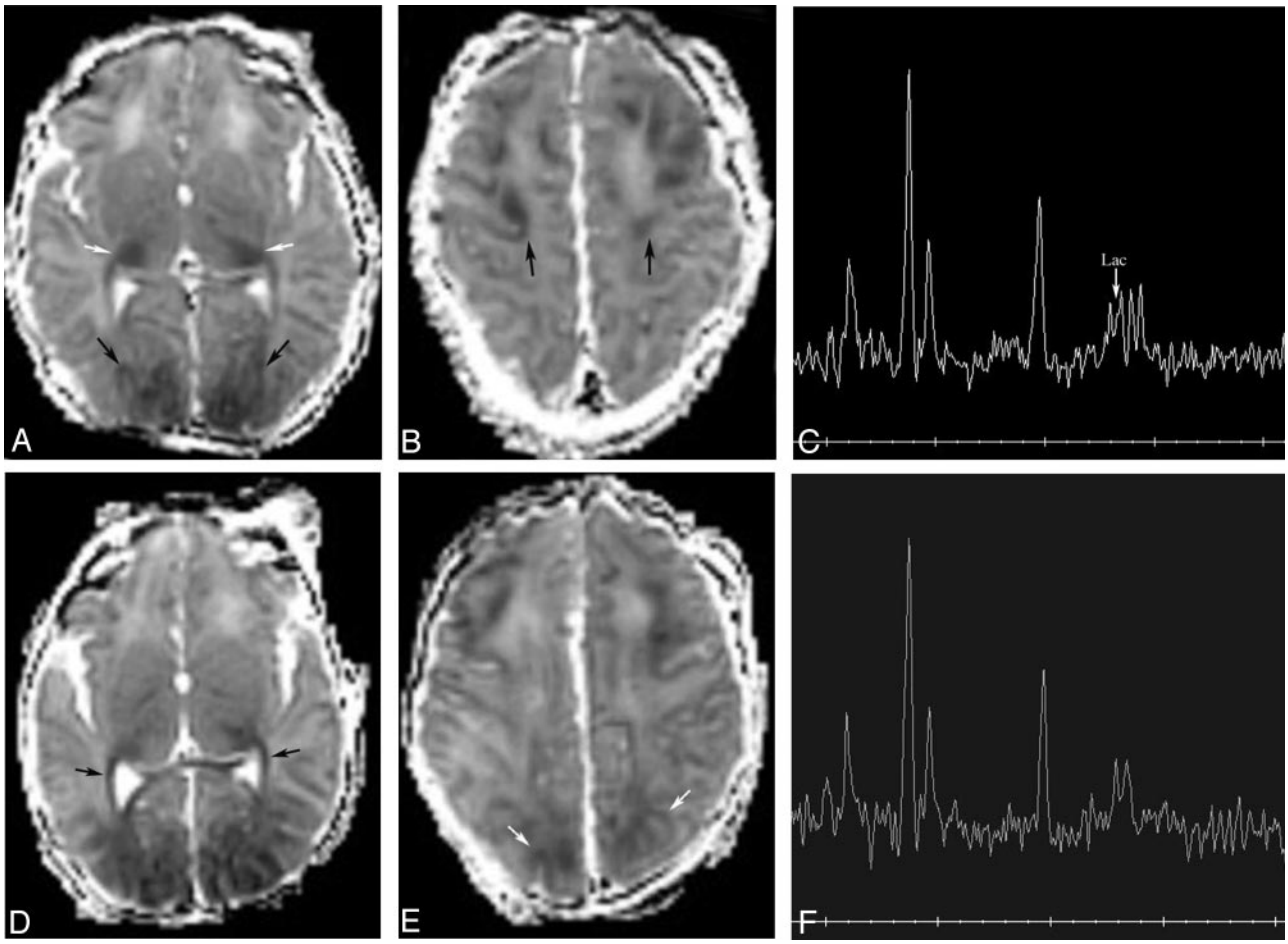

Fig 6. Patient 154. Increased volume of injury in vascular boundary zones from 2 to 4 days.

A and *B,* Axial D_{av} maps at 49 hours show reduced diffusivity (D_{av} reduced by about 20%, *black arrows*) in the frontal and parietooccipital intervascular boundary zones. Note also some reduced diffusivity in the posterolateral thalami (*white arrows*).

C, Proton MR spectroscopy from the left frontal white matter at 49 hours shows mild lactate (Lac) elevation.

D and *E,* Axial D_{av} maps at 91 hours show more extensive reduced diffusivity in the frontal and parieto-occipital intervascular boundary zones and new reduced diffusivity along the optic radiations (*black arrows*). D_{av} values were not significantly changed from the prior study at 49 hours.

F, Although the proton MR spectrum does not look significantly changed, measurements showed a 16% decrease in Lac/NAA and a 36% decrease in Lac/Ch in the frontal white matter compared with the study at 49 hours.

the changes, particularly in individual patients, has not been clarified. We report additional patients and spectroscopic results in an attempt to add to the limited knowledge on this subject in humans.

A number of interesting results emerge from this study. Probably the most interesting is the observation that both diffusivity and metabolic ratios are abnormal on the first or second day of life and then, in most patients, continue to worsen until the fourth or fifth day, after which they begin to normalize. For example, in patient 178 (who had a basal ganglia pattern of injury), D_{av} was about 0.85 mm^2/s and Lac/NAA was about 0.25 in the lateral thalami on day 1. By the second study on day 4, D_{av} was about 0.50 mm^2/s and Lac/NAA was about 0.9, but at the third study on day 8 D_{av} was about 0.95 mm^2/s and Lac/NAA was about 0.35. These patterns of evolution are similar to those seen in animal models.[41-45] Studies in infant pigs and rats have shown reduction in ADC[42-45] and impaired mitochondrial metabolism, with consequent increase in lactate and decrease in ATP[41,46] during ischemia. These values transiently partially normalize when normal cerebral blood flow and normoxia are restored, only to decrease again after 24–48 hours secondary to what is known as secondary energy failure.[47-49] Of interest, the most severely affected brain, that of patient 163, had very low D_{av} (about 0.40 mm^2/s) and very high Lac/NAA (1.7) in the thalami at the end of day 1 (22 hours after birth), which suggests that the normalization may not occur in all patients. This observation is consistent with that of Miyasaka et al,[43] who found that rats with the most severe injury never experienced recovery but progressed directly to cell necrosis and death. Indeed, the subsequent study of patient 163 revealed D_{av} of about 0.30 mm^2/s and Lac/NAA of 2.8 in the thalami, which shows a clear worsening. Another possible explanation, however, is that patient 163 suffered prenatal injury, as in utero seizures were detected 3 days before birth and a flat fetal heart rate was detected immediately before emergent caesarean section was performed. Thus, it is possible that the transient normalization of D_{av} and lactate occurred before delivery and that worst values may have occurred on day 2–3 after birth (which might have been day 4–5 after injury) instead of day 5 after birth. Unfortunately, a third study

could not be performed on this child because of the severity of the injury. Another patient in whom the pattern of evolution was somewhat atypical was patient 155, who had a cortical intravascular boundary zone injury after a history of oligohydramnios, thick meconium at birth, and neonatal depression. The pattern of evolution of D_{av} was typical for this patient, because the hemispheric voxels showed slight reduction of D_{av} on the first study (about 1.20 mm^2/s on day 1), more significant reduction on the second study (about 0.85 mm^2/s on day 6) and normalization (ranging from 1.20–1.60 mm^2/s on day 8) on the third study; however, Lac/NAA decreased from the first to the second to the third study, and most other ratios showed a similar unidirectional change from the first to the third study. This observation suggests that evolution of changes in metabolism, reflected in metabolite ratios, may have a different time course than those of microstructure, as reflected in D_{av}. It may also reflect differences in the temporal evolution of intravascular boundary zone injury as compared with deep gray matter injury, in addition to the severity of the hypoxic-ischemic insult. Further studies with larger cohorts will be necessary to determine the factors involved.

Absence of the normal hyperintensity in the posterior limb of the internal capsule on T1-weighted images has been described as a sensitive early (during the first week of life) sign of brain injury on MR imaging studies.[6] Therefore, because all members of our cohort were studied within 48 hours of birth, we specifically looked for this sign. Of interest, the normal hyperintensity was seen in all patients except 2. These 2 patients (patients 153 and 163) were born at gestational ages of 36 and 37 weeks, ages when myelination is not typically sufficient for this hyperintensity to be seen.[50,51] Thus, it appears that the absence of hypointensity in the posterior limb of the internal capsule, though helpful later in the first week of life, is not a sensitive sign for brain injury in the first 2 days after injury.

One very interesting observation of this study is that the pattern of reduced diffusion seemed to change over time on the sequential studies. This was much more dramatic in the patients with the basal ganglia pattern of injury; the pattern did not significantly change in the 2 patients with predominant watershed pattern. In the patients with basal ganglia pattern, the earliest studies showed reduced diffusion in only the ventrolateral thalami or the ventrolateral thalami and the more caudal aspects of the corticospinal tracts (Figs 2–5). Subsequent studies on days 3–5 showed reduced diffusion in the putamina and in the corticospinal tracts all the way to the perirolandic cortex (Figs 3 and 4). In addition, D_{av} maps on days 6 or 7 in several of the subjects showed reduced diffusion in the subcortical white matter and in white matter pathways such as the corpus callosum, the cingulum, and what appeared to be the fronto-occipital fasciculus (Fig 5) and the uncinate fasciculus. Moreover, the reduced diffusivity seemed to disappear in certain structures as it appeared in others, so that, for example, as diffusion in the thalami began to normalize, the white matter tracts and putamina began to show reduced diffusion. Consequently, on day 8, the diffusivity map of patient 178 showed reduced diffusivity of the posterior putamina with nearly normal ventrolateral thalami (Fig 4). Had this been the initial study, one might have suggested that the thalami had been spared; however, the diffusivity map from the initial study on day 1 had shown normal putamina and reduced diffusivity in the ventrolateral thalami (Fig 4). Awareness of this phenomenon is critical in the proper interpretation of these studies. Although McKinstry et al have described changes in diffusivity over time, noting that in their series D_{av} was maximally reduced (by about 35%) between days 2 and 3, and pseudonormalization of D_{av} was noted after the seventh day[21] they did not note evolution of the apparent pattern of injury. The reason for this evolution in the location of abnormal diffusivity may be a different susceptibility of different parts of the brain to injury, because this selective vulnerability has been suggested in the past as the reason that specific areas are sometimes injured in neonatal hypoxic-ischemic injury.[10,52] Another interesting possibility is raised by the observation of reduced diffusion in multiple white matter fascicles, however, perhaps this represents a type of excitotoxic injury spreading along the axons, or a variant of Wallerian degeneration that results from injury to the neuronal cell soma. Reduced diffusion in white matter tracts secondary to presumed Wallerian degeneration has been described after acute infarction in neonates and children. It is also important to note that the prolonged evolution of brain injury in this cohort is consistent with rodent models of hypoxic-ischemic injury in the immature brain, where cell death, particularly in the thalamus, progresses considerably during the first week after the insult.[54,55] Again, further studies with larger numbers of patients and, perhaps study of animal models with sequential MR evaluations will be necessary to answer these questions.

It is interesting to note that, though lactate levels in general increased to a maximum at 5–6 days and then diminished, Lac/NAA and Lac/Ch continued to be elevated in 2 patients at 7 (patient 193) and 14 days (patient 195), compared with levels on day 2 (see Table 3). Persistent lactate elevation >1 month after birth has been reported elsewhere after perinatal hypoxia-ischemia[56]) and postulated to be the result of persistent abnormal metabolism in the injured regions of brain. The patients in this study were examined at considerably younger ages. Therefore, it is not clear whether the relatively high values on the second scans might be the result of the initial studies (performed at 34 and 44 hours after birth) having sampled the brain tissues before or early in the course of secondary energy failure and, consequently before lactate values had become elevated. Another factor in patient 193 might be the severity of the injury, which may have resulted in longer persistence of lactate elevation. The case of patient 195 is interesting and deserves further discussion. This patient barely qualified for entry into our study, with a somewhat low arterial pH of 7.08. He was admitted to the well-baby nursery, where he was noted to be "jittery" and to have mild hypoglycemia but was otherwise judged to be completely healthy. The initial MR study was normal and the baby was discharged home as a normal neonate; the follow-up MR was scheduled as an outpatient. Because of various complications in the schedules of the MR scanner and the parents, the follow-up MR study was not performed until day 14 of life. Results at that time showed a new, unexpected abnormality in the right frontal white matter and an interval increase in lactate in the cerebral white matter. Neurodevelopmental examination at age 3 months found the infant to be completely normal. These findings raise the interesting possibility that even "normal" neonates can suffer mild

brain injuries in the perinatal and neonatal periods. The long-term consequences of such injuries are unknown. Perhaps more information on such situations will come from the ongoing NIH-supported development of a data base of MR imaging parameters of the brains of normal infants.[57]

One very important question that should be asked in any study of neonatal encephalopathy is which findings are associated with poor outcomes and which are associated with good outcomes. Unfortunately, the limited number of patients in this study does not permit any definite conclusions in this regard. Moreover, several of our patients had very severe brain injuries and did not survive to undergo follow-up examinations. Many of our subjects had D_{av} values below the threshold of 0.75 mm^2/s suggested by Hunt et al[22] as an objective prognostic marker for infants with brain injury.

This study is hampered by a number of limitations that are characteristic of all studies of sick neonates in busy hospitals. Although attempts were made to study all of the patients at regular times, this goal was not achieved. Initially, it was the intention of this project to study all the neonates in the first 24 hours after birth; unfortunately, it is nearly impossible to transport neonates born at outlying hospitals to our institution, stabilize them, mobilize them for an MR study, and study them safely in such a short timeframe. Therefore, fewer than half of the subjects were studied within 24 hours, with the remainder being studied between 24 and 48 hours. An attempt was made to perform the follow-up scans at variable times 3–6 days after birth, to understand the evolution of MR parameters over that time period. This was achieved reasonably well, though scheduling difficulties resulted in many patients being scanned at slightly different time intervals than hoped. The most extreme example of this was the child in our cohort with the least severe neonatal course (patient 195), whose follow-up MR (as an outpatient) did not occur until 14 postnatal days. Two patients were imaged 3 times, giving the best pictures of the evolution of the brain injury. It is hoped that as more neonates are enrolled into the study, the large number of patients studied will compensate for the varying times and allow an even clearer picture of evolving injury to emerge. In an ideal environment, single patients could be studied more frequently (every other day, for example), but in most institutions the time involved in multiple transports to and from the scanner and paucity of scanner time make this very difficult, if not impossible.

Another limitation of this study is common to nearly all studies of neonatal encephalopathy, that precise time of injury was not known in most of the patients. Indeed, as discussed above, one of the patients appeared to develop seizures in utero, 3 days before delivery, and was presumed to have prenatal injury. Another had oligohydramnios and thick meconium present at delivery, which suggest possible prenatal injury. Furthermore, different patterns of injury were seen in the different patients. Two appeared to have mostly cortical damage, in the intervascular boundary zones (watershed regions), whereas 5 had predominant deep gray matter injury and 2 had extensive injury in both cortex and deep gray matter. The timing of evolution may well be different in different injury patterns. Finally, the evolution may differ in injuries of differing severity and causality, even if the pattern is the same. This underscores the importance of serial studies in an individual neonate to clarify these issues.

Despite these limitations, this study provides important information for the MR evaluation of encephalopathic neonates. The extent and pattern of injury vary temporally. Particularly in the case of proton spectroscopy and DTI, some areas will appear more severely injured and some less injured, depending on the timing of the scan with respect to the injury. Most important, early studies often underestimate the ultimate extent of damage, even if diffusion and spectroscopy are included. Because it appears from these data that injury is still evolving, it will be interesting to determine, in future studies, whether interventions can reduce or prevent such progression of injury.

References

1. Groenendaal F, Veenhoven EH, van der Grond J, et al. **Cerebral lactate and *N*-acetyl-aspartate/choline ratios in asphyxiated full-term neonates demonstrated in-vivo using proton magnetic resonance spectroscopy.** *Pediatr Res* 1994;35:148–51
2. Preden CJ, Rutherford MA, Sargentoni J, et al. **Proton spectroscopy of the neonatal brain following hypoxic-ischemic injury.** *Dev Med Child Neurol* 1993;35:502–10
3. Bryant DJ, Sargentoni J, Cox IJ, et al. **Proton magnetic resonance spectroscopy of term infants with hypoxic ischaemic injury.** In: *Proceedings of the Society of magnetic resonance.* San Francisco;1994;336
4. Hanrahan JD, Sargentoni J, Azzopardi D, et al. **Cerebral metabolism within 18 hours of birth asphyxia: a proton magnetic resonance spectroscopy study.** *Pediatr Res* 1996;39:584–90
5. Rutherford M, Pennock J, Schwieso J, et al. **Hypoxic ischaemic encephalopathy: early and late magnetic resonance findings in relation to outcome.** *Arch Dis Child Fetal Neonatal Ed* 1996;75:F145–F151
6. Rutherford M, Pennock J, Schwieso JE, et al. **Hypoxic-ischemic encephalopathy: early magnetic resonance imaging findings and their evolution.** *Neuropediatrics* 1995;26:183–91
7. Robertson R, Ben-Sira L, Barnes P, et al. **MR line scan diffusion weighted imaging of term neonates with perinatal brain ischemia.** *AJNR Am J Neuroradiol* 1999;20:1658–70
8. Barnett A, Mercuri E, Rutherford M, et al. **Neurological and perceptual-motor outcome at 5–6 years of age in children with neonatal encephalopathy: relationship with neonatal brain MRI.** *Neuropediatrics* 2002;33:242–48
9. Cowan F, Rutherford M, Groenendaal F, et al. **Origin and timing of brain lesions in term infants with neonatal encephalopathy.** *Lancet* 2003;361:736–42
10. Barkovich AJ. **MR and CT evaluation of profound neonatal and infantile asphyxia.** *AJNR Am J Neuroradiol* 1992;13:959–72
11. Barkovich AJ, Baranski K, Vigneron D, et al. **Proton MR spectroscopy in the evaluation of asphyxiated term neonates.** *AJNR Am J Neurorad* 1999;20:1399–405
12. Barkovich AJ, Sargent SK. **Profound asphyxia in the preterm infant: imaging findings.** *AJNR Am J Neuroradiol* 1995;16:1837–46
13. Barkovich AJ, Westmark KD, Ferriero DM, et al. **Perinatal asphyxia: MR findings in the first 10 days.** *AJNR Am J Neuroradiol* 1995;16:427–38
14. Barkovich AJ, Westmark KD, Bedi HS, et al. **Proton spectroscopy and diffusion imaging on the first day of life after perinatal asphyxia: preliminary report.** *AJNR Am J Neuroradiol* 2001;22:1786–94
15. Sie L, van der Knaap M, van Wezel-Meijler G, et al. **Early MR features of hypoxic-ischemic brain injury in neonates with periventricular densities on sonograms.** *AJNR Am J Neuroradiol* 2000;21:852–61
16. Krägeloh-Mann I, Helber A, Mader I, et al. **Bilateral lesions of thalamus and basal ganglia: origin and outcome.** *Dev Med Child Neurol* 2002;44:477–84
17. Pasternak JF, Gorey MT. **The syndrome of acute near total intrauterine asphyxia in the term infant.** *Pediatr Neurol* 1998;18:391–98
18. Roland EH, Poskitt K, Rodriguez E, et al. **Perinatal hypoxic-ischemic thalamic injury: clinical features and neuroimaging.** *Ann Neurol* 1998;44:161–66
19. Wolf RL, Zimmerman RA, Clancy R, et al. **Quantitative apparent diffusion coefficient measurements in term neonates for early detection of hypoxic-ischemic brain injury: initial experience.** *Radiology* 2001;218:825–33
20. Rutherford M, Counsell S, Allsop J, et al. **Diffusion weighted magnetic resonance imaging in term perinatal brain injury: a comparison with site of lesion and time from birth.** *Pediatrics* 2004;114:1004–14
21. McKinstry R, Miller J, Snyder A, et al. **A prospective, longitudinal diffusion tensor imaging study of brain injury in newborns.** *Neurology* 2002;59:824–33
22. Hunt RW, Neil JJ, Coleman LT, et al. **Apparent diffusion coefficient in the**

posterior limb of the internal capsule predicts outcome after perinatal asphyxia. *Pediatrics* 2004;114:999–1003
23. Hüppi PS, Murphy B, Maier SE, et al. **Microstructural brain development after perinatal cerebral white matter injury assessed by diffusion tensor magnetic resonance imaging.** *Pediatrics* 2001;107:455–60
24. Barkovich AJ, Hajnal BL, Vigneron D, et al. **Prediction of neuromotor outcome in perinatal asphyxia: evaluation of MR scoring systems.** *AJNR Am J Neuroradiol* 1998;19:143–50
25. Mercuri E, Atkinson J, Braddick O, et al. **Visual function in full-term infants with hypoxic-ischemic encephalopathy.** *Neuropediatrics* 1997;28:155–61
26. Mercuri E, Haataja L, Guzzetta A, et al. **Visual function in term infants with hypoxic-ischaemic insults: correlation with neurodevelopment at 2 years of age**. *Arch Dis Child Fetal Neonatal Ed* 1999;80:F99–104
27. Mercuri E, Rutherford M, Cowan F, et al. **Early prognostic indicators of outcome in infants with neonatal cerebral infarction: a clinical, electroencephalogram, and magnetic resonance imaging study.** *Pediatrics* 1999;103:39–46
28. Miller SP, Newton N, Ferriero DM, et al. **Predictors of 30-month outcome following perinatal depression: role of proton MRS and socio-economic factors.** *Pediatr Res* 2002;52:71–77
29. Miller SP, Ramaswamy V, Michelson D, et al. **Patterns of brain injury in term neonatal encephalopathy.** *J Pediatr* 2005;146:453–60
30. Ferriero DM. **Neonatal brain injury.** *N Engl J Med* 2004;351:1985–95
31. Taylor DL, Mehmet H, Cady EB, et al. **Improved neuroprotection with hypothermia delayed by 6 hours following cerebral hypoxia-ischemia in the 14-day-old rat.** *Pediatr Res* 2002;51:13–19
32. Vannucci RC, Perlman JM. **Interventions for perinatal hypoxic-ischemic encephalopathy.** *Pediatrics* 1997;100:1004–14
33. Dumoulin CL, Rohling KW, Piel JE, et al. **Magnetic resonance imaging compatible neonate incubator.** *Concept Magne Reson (Magn Reson Eng)* 2002;15:117–28
34. Maas L, Mukherjee P, Carballido-Gamio J, et al. **Early laminar organization of the human cerebrum demonstrated with diffusion tensor imaging in extremely premature infants.** *Neuroimage* 2004;22:1134–40
35. Partridge SC, Mukherjee P, Henry R, et al. **Diffusion tensor imaging: serial quantitation of white matter tract maturity in premature newborns.** *Neuroimage* 2004;22:1302–14
36. DeIpolyi AR, Mukherjee P, Gill K, et al. **Comparing microstructural and macrostructural development of the cerebral cortex in premature newborns: diffusion tensor imaging versus cortical gyration.** *Neuroimage* 2005;27:579–86
37. Vigneron DB, Barkovich AJ, Noworolski SM, et al. **Three-dimensional proton MR spectroscopic imaging of premature and term neonates.** *AJNR Am J Neuroradiol* 2001;22:1424–33
38. Pauly J, Le Roux P, Nishimura D, et al. **Parameter relations for the Shinnar-Le Roux selective excitation pulse design algorithm.** *IEEE Trans Med Imaging* 1991;10:53–65
39. Kreis R, Ernst T, Ross BD. **Development of the human brain: *in vivo* quantification of metabolite and water content with proton magnetic resonance spectroscopy.** *Mag Res Med* 1993;30:424–37
40. Hanrahan JD, Cox IJ, Azzopardi D, et al. **Relation between proton magnetic resonance spectroscopy within 18 hours of birth asphyxia and neurodevelopment at 1 year of age.** *Dev Med Child Neurol* 1999;41:76–82
41. Penrice J, Lorek A, Cady EB, et al. **Proton magnetic resonance spectroscopy of the brain during acute hypoxia-ischemia and delayed cerebral energy failure in the newborn piglet.** *Pediatr Res* 1997;41:795–802
42. Thornton JS, Ordidge RJ, Penrice J, et al. **Anisotropic water diffusion in white and gray matter of the neonatal piglet brain before and after transient hypoxia-ischaemia.** *Magn Res Imag* 1997;15:433–40
43. Miyasaka N, Kuroiwa T, Zhao FY, et al. **Cerebral ischemic hypoxia: discrepancy between apparent diffusion coefficients and histologic changes in rats.** *Radiology* 2000;215:199–204
44. Miyasaka N, Nagaoka T, Kuriowa T, et al. **Histopathologic correlates of temporal diffusion changes in a rat model of cerebral hypoxia/ischemia.** *AJNR Am J Neuroradiol* 2000;21:60–66
45. Qiao M, Malisza KL, Del Bigio MR, et al. **Transient hypoxia-ischemia in rats: changes in diffusion-sensitive MR imaging findings, extracellular space, and Na+-K+ adenosine triphosphatase and cytochrome oxidase activity.** *Radiology* 2002;223:65–75
46. Nedelcu J, Klein MA, Aguzzi A, et al. **Biphasic edema after hypoxic-ischemic brain injury in neonatal rats reflects early neuronal and late glial damage.** *Pediatr Res* 1999;46:297–304
47. Hope PL, Costello AM, Cady EB, et al. **Cerebral energy metabolism studied with phosphorus NMR spectroscopy in normal and birth-asphyxiated infants.** *Lancet* 1984;2:366–70
48. Azzopardi D, Wyatt JS, Cady EB, et al. **Prognosis of newborn infants with hypoxic-ischemic injury assessed by phosphorus magnetic resonance spectroscopy.** *Pediatr Res* 1989;25:445–51
49. Lorek A, Takei Y, Cady EB, et al. **Delayed ("secondary") cerebral energy failure after acute hypoxia-ischemia in the newborn piglet: continuous 48-hour studies by phosphorus magnetic resonance spectroscopy.** *Pediatr Res* 1994;36:699–706
50. Sie LTL, van der Knaap MS, van Wezel-Meijler G, et al. **MRI assessment of myelination of motor and sensory pathways in the brain of preterm and term born infants.** *Neuropediatrics* 1997;28:97–105
51. Counsell S, Maalouf E, Fletcher A, et al. **MR imaging assessment of myelination in the very preterm brain.** *AJNR Am J Neuroradiol* 2002;23:872–81
52. McQuillen PS, Ferriero DM. **Selective vulnerability in the developing central nervous system.** *Pediatr Neurol* 2004;30:227–35
53. Mazumdar A, Mukherjee P, Miller J, et al. **Diffusion-weighted imaging of acute corticospinal tract injury preceding Wallerian degeneration in the maturing human brain.** *AJNR Am J Neuroradiol* 2003;24:1057–66
54. Northington FJ, Ferriero DM, Flock DL, et al. **Delayed neurodegeneration in neonatal rat thalamus after hypoxia-ischemia is apoptosis.** *J Neurosci* 2001;21:1931–38
55. Northington FJ, Ferriero DM, Graham EM, et al. **Early neurodegeneration after hypoxia-ischemia in neonatal rat is necrosis while delayed neuronal death is apoptosis.** *Neurobiol Dis* 2001;8:207–19
56. Hanrahan JD, Azzopardi D, Cowan FM, et al. **Persistent increases in cerebral lactate concentration after birth asphyxia.** *Pediatr Res* 1998;44:304–11
57. McKinstry RC and the NIH Brain Development Cooperative Group. **MR imaging study of normal brain development.** Presented at: 13th Annual Meeting of the International Society of Magnetic Resonance in Medicine, Miami, Fla., May 7-13, 2005